Vibrational Normal Modes of Small Thiolate-Protected Gold Clusters

ARTICLE *in* THE JOURNAL OF PHYSICAL CHEMISTRY C · JUNE 2013

Impact Factor: 4.77 · DOI: 10.1021/jp4033063

3 AUTHORS, INCLUDING:

Alfredo Tlahuice-Flores
University of Texas at San Antonio
25 PUBLICATIONS **262** CITATIONS
SEE PROFILE

Miguel Jose Yacaman
University of Texas at San Antonio
467 PUBLICATIONS **10,497** CITATIONS
SEE PROFILE

THE JOURNAL OF PHYSICAL CHEMISTRY C

Article

pubs.acs.org/JPCC

Vibrational Normal Modes of Small Thiolate-Protected Gold Clusters

Alfredo Tlahuice-Flores,* Robert L. Whetten, and Miguel Jose-Yacaman

Department of Physics and Astronomy, University of Texas at San Antonio, One UTSA Circle, San Antonio, Texas 78249, United States

Supporting Information

ABSTRACT: This report addresses a density functional theory study of the vibrational normal modes of small-sized thiolate-protected gold clusters. Calculated far-infrared (far-IR) and low-frequency Raman spectra of established thiolate-protected gold clusters (4, 12, 18, 19, 20, 24, and 25 Au atoms) show characteristic peaks in the range of 20−350 cm^{-1} that can be attributed to the breathing mode of the gold core, Au−S−Au bending modes and Au−S stretching modes. It was found that as cluster size increases the Au_{13} breathing mode of Au_{25} cluster emerges. This study reveals both systematic and specific characteristics that may provide a basis for identification ("fingerprinting") by far-IR and low-frequency Raman spectroscopy of the many diverse gold−thiolate cluster compounds.

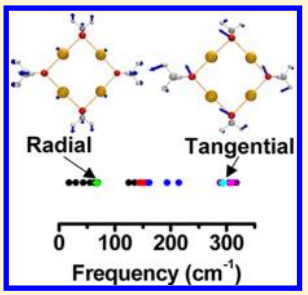

1. INTRODUCTION

The study of thiolate-protected gold clusters and their astonishing properties due to their reduced size is part of intense research nowadays. Their potential applications include antiarthritic and antitumor drugs and their use in catalysis.[1,2] Thiolate-protected gold clusters consist of a single gold core covered by RS-Au-RS (monomer), RS-Au-RS-Au-RS (dimer), and RS-Au-RS-Au-RS-Au-RS (trimer) motifs, where R is a ligand group, which can be termed staple motifs. Because of the existence of gold adatoms forming part of mentioned staple motifs, in the structure of thiolate-protected gold clusters one may distinguish between two types of gold atoms, those forming part of the core (Au(core)) and those included in the staples motifs (Au(staple)). The first total X-ray determined structure of the $Au_{102}(SR)_{44}$ cluster by the Kornberg group in 2007 determined one Au_{79} core protected by 19 monomer and 2 dimer motifs.[3] After that, crystallization of the $Au_{25}(SR)_{18}^{-}$ cluster shows a structure based on one symmetric Au_{13} core protected with six dimer motifs; since its structural prediction and crystallization it has opened a fascinating field owing to its size-dependent properties.[4−6] Another amply studied $Au_{38}(SR)_{24}$ cluster is built by an elongated Au_{23} core and six dimer and three monomer motifs.[7,8] In a recent paper by Pei et al., other thiolate-protected cluster sizes are reviewed and included in this study.[9]

It is well known that vibrational properties are a manner of structural characterization, and a great number of reports present the infrared (IR) and Raman spectra covering the mid-IR range, corresponding to modes with a fundamental frequency of 350−3500 cm^{-1}. These modes are localized in the organic tail-group (R-), allowing one to establish that it remains intact; the R-group conformation and ordering may also be deduced from the details of such spectra. Unfortunately, this region is notoriously insensitive to the structure and bonding in the headgroup region, that is, the Au−S bonding network, as well as to the Au−Au modes of the core. The structurally relevant modes appear instead in the far-IR (20−350 cm^{-1}) and the corresponding low-frequency Raman spectral regions. In this direction, the Fielicke group in 2008 was able to measure IR spectrum of a tetrahedral Au_{20} cluster, among others, in the gas phase.[10] Regarding thiolate-protected gold clusters, the measurement of the breathing mode of anionic $Au_{25}(SR)_{18}$ cluster by solid-state Raman experiments has been previously reported by the Murray group.[11] Up to the present, a significant portion of the available data is due to experimental work with a few attempts of theoretical study of vibrational properties of thiolate-protected gold clusters.[12−17]

In this report is addressed the study of the vibrational normal modes of well-established structures of small thiolate-protected gold clusters by means of density functional theory (DFT) calculations. This study focuses on the calculation of IR and Raman spectra of thiolate-protected gold clusters, composed of up to 25 Au atoms and 18 thiolate ligands to determine features of their vibrational spectra and how their spectra depend on the cluster size and composition and structure. We are unaware of any previous systematic exploration of the low-frequency spectra; therefore, a prime objective of this research is to correlate the spectral features to the various structure and bonding characteristics, and correlation may establish the "fingerprinting" potential of far-IR/low-frequency Raman spectroscopy for the rapid spectral identification of these and many related compounds.

2. THEORETICAL METHOD

The vibrational normal modes were obtained by means of DFT calculations with generalized gradient approximation (GGA). The PBE functional and LANL2DZ (19 valence electrons) were employed for Au atoms and 6-31G(d,p) basis set for S, C,

Received: April 3, 2013
Revised: May 15, 2013
Published: May 17, 2013

   dx.doi.org/10.1021/jp4033063 | J. Phys. Chem. C 2013, 117, 12191−12198

and H atoms.[18] The basis set used includes diffuse functions for a more approximate prediction of intensities.[19a] Structural optimizations were performed using a force tolerance criterion of 0.01 eV/Å. Well-established structures of thiolate-protected gold clusters incorporating $-SCH_3$ as ligands were fully relaxed, and their harmonic frequencies were calculated using the same level of theory. Plots of calculated IR and Raman spectra employ a Gaussian line shape with a broadening of 5 cm^{-1}, while calculated intensities are represented as colored sticks (Figures 1 and 2). All mentioned methodology is implemented

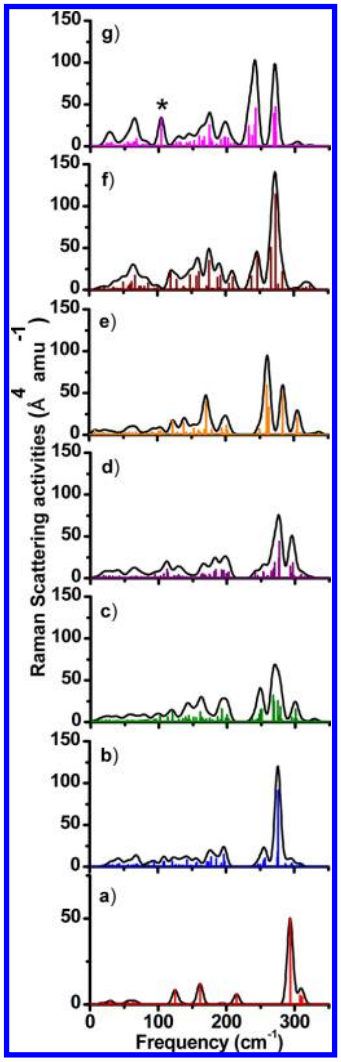

Figure 1. Calculated Raman spectra with intensities represented as colored sticks. (a) $Au_4(SCH_3)_4$, (b) $[Au_{12}(SCH_3)_9]^+$, (c) $Au_{18}(SCH_3)_{14}$, (d) $Au_{19}(SCH_3)_{13}$, (e) $Au_{20}(SCH_3)_{16}$, (f) $Au_{24}(SCH_3)_{20}$, and (g) $[Au_{25}(SCH_3)_{18}]^-$. More intense breathing mode of the $[Au_{25}(SCH_3)_{18}]^-$ cluster is labeled with an asterisk.

in the Gaussian 03 package.[20] This methodology has been previously used in the prediction of IR spectrum of the anionic $Au_{25}(SR)_{18}$ cluster, finding good agreement with experiments and other calculations.[17]

In this report, only the harmonic frequencies are given, and they will require correction using the corresponding scale factor, as indicated in ref 19b to correlate them with the experimental data. The reported scale factor in the low-frequency range for the PBE functional and the 6-31G (d,p)

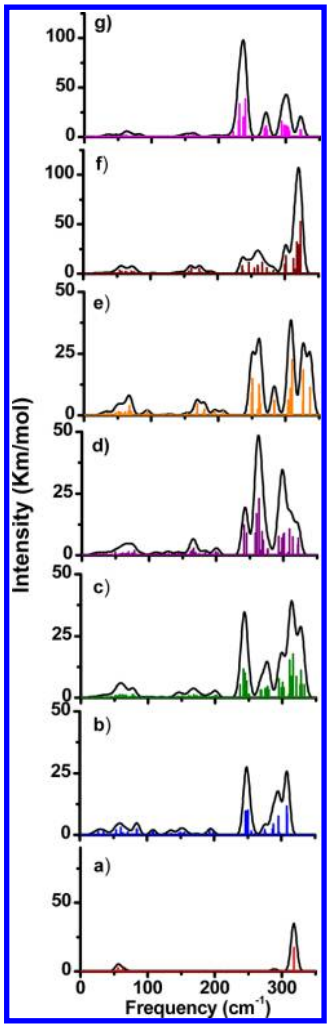

Figure 2. Infrared spectra of calculated clusters. (a) $Au_4(SCH_3)_4$, (b) $[Au_{12}(SCH_3)_9]^+$, (c) $Au_{18}(SCH_3)_{14}$, (d) $Au_{19}(SCH_3)_{13}$, (e) $Au_{20}(SCH_3)_{16}$, (f) $Au_{24}(SCH_3)_{20}$, and (g) $[Au_{25}(SCH_3)_{18}]^-$.

basis set is given as 1.0539 in the mentioned paper by Merrick et al.

All studied clusters were obtained from reported structures and relaxed using the methodology mentioned above. We are primarily considering the ligand $-SCH_3$ in this report, which can be justified as follows. For the $Au_4(SCH_3)_4$ cluster and the anionic $Au_{25}(SCH_3)_{18}$ cluster, we have relaxed the structures that include R = −SH, $-SCH_3$, and $-SCH_2CH_2Ph$ as ligands to compare the bond lengths (Au(core)−Au(core)), Au-(core)−S, Au(staple)−S, and S−C). (See Figures S3 and S4 in the Supporting Information.) Our structural analysis establishes a close correspondence of these bond parameters across the mentioned ligands, which gives us some confidence to expect similar Au−S vibrations within the range of systems studied. We also calculated selected vibrational frequencies (breathing modes) for a limited range of small (tetramer) and larger ($Au_{25}R_{18}^-$) clusters, with results displayed in Table S1 in the Supporting Information. These results establish a close correspondences of the important low-frequency modes across the various ligand types. These core breathing modes, which are prominent among those detected experimentally, are characteristic of the core size.[11,41]

dx.doi.org/10.1021/jp4033063 | J. Phys. Chem. C 2013, 117, 12191−12198

3. RESULTS AND DISCUSSION

In the following, each cluster size is discussed regarding its structural and vibrational properties, and finally the obtained trends are summarized.

3.1. $Au_4(SCH_3)_4$ Cluster. Thiolate-protected gold clusters following the proportion 1:1 between ligands and gold atoms have been observed experimentally. They are considered to have no direct metal−metal bonding and are sometimes referred to as aurous, or Au(I), thiolate oligomers[21−23] The structure of the $Au_4(SCH_3)_4$ cluster has been previously calculated in refs 24−26 as a cyclic structure. In this report, a more stable structure of $Au_4(SCH_3)_4$ was found as a D_{2d} point group, and its structure shows 24 bonds that are distributed as follows: 12 C−H bonds (1.1 Å), 4 S−C bonds (1.85 Å), and 8 Au−S bonds (2.37 Å). The interatomic Au−Au distance was determined to be 3.37 Å. The obtained bond lengths are in agreement with those reported study by Cliffel et al. that also used PBE approximation.[25] However, even when the same PBE functional was used in the ref 24b, our calculated Au−S bond distances were slightly larger than those reported there, and the Au−S vibration is accordingly lower, as will be shown below.

The $Au_4(SCH_3)_4$ cluster holds a D_{2d} symmetry, and its 66 normal modes are classified in the irreducible representation $\Gamma = 9A_1 + 8A_2 + 9B_1 + 8B_2 + 16E$, where B_2 and E are Raman- and IR-active, and A_1 and B_1 are Raman-active.

Its calculated Raman spectrum (Figure 1a) shows four major peaks in the range 18−350 cm^{-1}; a symmetric Au−S stretching mode of ligands produces an intense peak at 293.3 cm^{-1} (A_1), while the breathing mode of the whole structure is weak and located at 67.7 cm^{-1} (A_1) (Table 1). The corresponding IR spectrum of $Au_4(SCH_3)_4$ cluster (Figure 2a), is dominated by two-fold degenerate peaks located at 317.7 and 55.8 cm^{-1},which may be described, respectively, as the asymmetric Au−S stretching mode and an S−CH_3 bending mode (with participation from S−Au−S bending). The vibration mode located at 317.7 cm^{-1} represents a "tangential" mode (Figure 3d), while breathing modes located at 67.7 and 293.3 cm^{-1} (Figure 3b,c) are directed radially with respect to the molecule center. In general, 12 weak IR Au−S−Au bending modes are included in the range 18.4−135.2 cm^{-1}; 5 torsional methyl modes are found in the range 143.9−155.4; 4 additional S-CH_3 bending modes or Au−S−Au bending modes are included in the range 161.22−214.8 cm^{-1}; and 8 Au−S stretching modes span the range 288−350 cm^{-1}. It is important to mention that $Au_4(SCH_3)_4$ represents a simple structure from which normal modes are feasibly distinguished; therefore, a study of its vibrational normal modes is mandatory.

Table 1. Raman Active Modes of Studied Clusters

structure	intense breathing mode of staple motifs, cm^{-1}	breathing mode of the core, cm^{-1}
$Au_4(SCH_3)_4$	293.30	67.70
$[Au_{12}(SCH_3)_9]^+$	275.90	94.50
$Au_{18}(SCH_3)_{14}$	267.20	105.10
$Au_{19}(SCH_3)_{13}$	277.60	112.40
$Au_{20}(SCH_3)_{16}$	259.90	101.70
$Au_{24}(SCH_3)_{20}$	273.0	86.30
$[Au_{25}(SCH_3)_{18}]^-$	268.60	103.80

3.2. Cationic $Au_{12}(SCH_3)_9$. The structure of cationic $Au_{12}(SR)_9$ cluster was first proposed by Jiang et al. and synthesized by the Choi group.[27,28] The originally proposed structure was a loose C_3 symmetry (0.07 Å tolerance), but in this study attempts to relax that point group were not successful and a C_1 structure was calculated. The $[Au_{12}(SCH_3)_9]^+$ cluster features 72 bonds in the range of 1.1 to 3.0 Å which includes, besides the 27 C−H bonds (1.1 Å) and 9 S−C bonds (1.85 Å), 12 Au("adatom" or staple)−S bonds (2.40 Å); 6 Au(core)−S bonds (2.46 Å) that link the dimer motifs to the Au_6 core; 12 Au(core)−Au(core) bonds (2.77 to 2.97 Å) forming the Au_6 core; as well as 6 Au(core)−Au(dimer) unusually short contacts (2.91 to 2.92 Å). It is important to notice that Au(dimer)−S(dimer) bonds are slightly shorter than the Au(core)−S(dimer) bonds that are linking dimer motifs to the Au_6 core (Figure S1 and S2 in the Supporting Information). The Au−Au bond lengths and average Au(core)−S distances were found to be in agreement with previous calculations.[29]

The $[Au_{12}(SCH_3)_9]^+$ cluster exhibits C_1 symmetry and 165 non-degenerate vibrational normal modes. Figure 1b shows its calculated Raman spectrum with a dominant peak located at 275.9 cm^{-1}, which is related to the breathing of the dimer motifs (Figure 4b shows the apical S atoms moving radially), while breathing mode of the Au_6 core may be identified at 94.5 cm^{-1}. The IR spectrum shows an intense peak at 246.1 cm^{-1} due to a radial Au(core)−S(dimer) stretching mode (Figure 4a). Other strong features are found at 295.7 cm^{-1}, an asymmetric Au−S stretching mode on dimer motifs (Figure 4c), and at 307.8 cm^{-1} (Figure 4d), a tangential Au(dimer)−S(dimer) mode.

The distribution of the vibrational normal modes of the $[Au_{12}(SCH_3)_9]^+$ cluster is as follows: The range 19−109 cm^{-1} is dominated by weak Au−S−Au bending modes, while they are more intense at 155−198 cm^{-1} and combined with S-CH_3 bending modes. Methyl torsional modes are found in the range 120−153 cm^{-1}, and Au−S stretching modes are included in the range 246−309 cm^{-1}.

3.3. $Au_{18}(SCH_3)_{14}$ Cluster. This cluster was identified initially by Tsukuda and coworkers and more recently by the Dass group, who use a surfactant-free method.[30−33] Its structure was proposed in 2012 on the basis of calculations of optical and chiroptical properties in agreement with prior

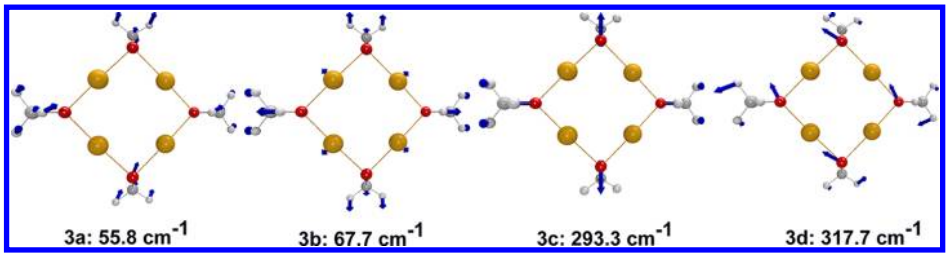

Figure 3. Selected vibrational normal modes of the $Au_4(SCH_3)_4$ cluster. S, C, H, and Au atoms are red, gray, white, and light brown, respectively.

dx.doi.org/10.1021/jp4033063 | J. Phys. Chem. C 2013, 117, 12191−12198

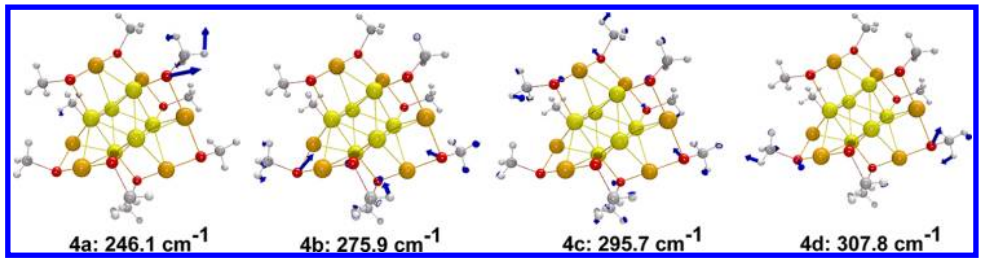

Figure 4. Selected vibrational normal modes of the $[Au_{12}(SCH_3)_9]^+$ cluster. S, C, H, Au(core), and Au(staple) atoms are red, gray, white, yellow, and light brown, respectively.

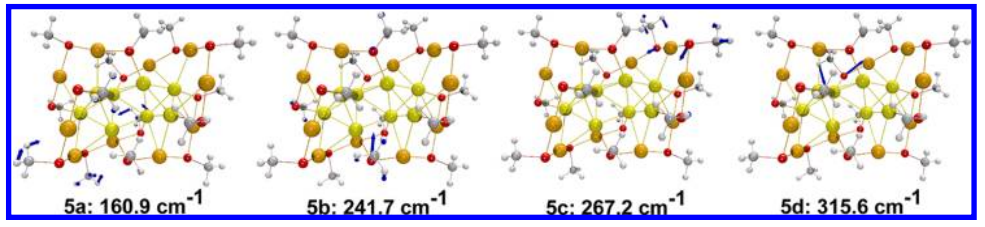

Figure 5. Selected vibrational normal modes of the $Au_{18}(SCH_3)_{14}$ cluster. S, C, H, Au(core), and Au(staple) atoms are red, gray, white, yellow, and light brown, respectively.

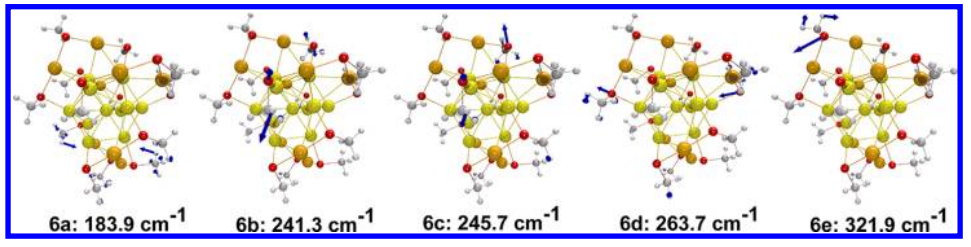

Figure 6. Selected vibrational normal modes of the $Au_{19}(SCH_3)_{13}$ cluster. S, C, H, Au(core), and Au(staple) atoms are in red, gray, white, yellow, and light brown, respectively.

experimental spectra.[34] The $Au_{18}(SCH_3)_{14}$ structure consists of an Au_8 core that can be seen as two displaced tetrahedral Au_4 subunits with a relative rotation and translation between them. Because of the mutual arrangement of the two dimer and two trimer motifs covering the Au_8 core, it is intrinsically chiral with a C_1 total symmetry. Structurally the $Au_{18}(SCH_3)_{14}$ cluster is built by bonds in the range 1.1 to 3.1 Å that are distributed as follow: 42 C−H bonds (1.1 Å), 14 S−C bonds (1.85 Å), 20 Au(staple)−S bonds (2.36−2.39 Å), 8 Au(core)−S bonds (2.44−2.47 Å), 10 Au(core)−Au(staple) bonds around 3.0 Å, and 15 Au(core)−Au(core) bonds included in the range 2.75 to 3.0 Å (six from each tetrahedron plus three linking them). From these calculated bond distances we conclude that $[Au_{12}(SCH_3)_9]^+$ and $Au_{18}(SCH_3)_{14}$ cluster have similar Au−S bonds but distinct Au−Au bond distances. In Figure S2 in the Supporting Information is shown the $Au_{18}(SCH_3)_{14}$ cluster that holds a distorted Au_8 core, as can be verified by its Au−Au bonds included in a wide range.

The $Au_{18}(SCH_3)_{14}$ cluster exhibits 258 normal modes that are Raman- and IR-active. The low-frequency range has a rich fine structure with the following prominent characteristics. The Raman spectrum (Figure 1c) shows a strong feature near 270 cm^{-1}, arising from modes including the one at 267.2 cm^{-1} (Figure 5c) related to the breathing of staple motifs; another well-defined feature is at 160.9 cm^{-1} (Figure 5a) attributed to S−CH_3 bending modes. The breathing mode of Au_8 core is found near 101.5 cm^{-1}, near the breathing mode of the $Au_{20}(SCH_3)_{16}$ cluster (vide infra). Noteworthy among the obtained features of the IR spectrum is the finding that Au(core)−S(staple) stretching modes of dimer motifs are located around 241.7 cm^{-1} (Figure 5b), while in trimer motifs these modes are located around 315.6 cm^{-1} (Figure 5d).

In general, in the $Au_{18}(SCH_3)_{14}$ cluster, weak Au−S−Au bending modes are distributed up to 109 cm^{-1}, and they are mixed with weak IR methyl torsional modes in the range 112−172 cm^{-1}. Slightly more intense IR- and Raman-active Au−S−Au bending modes are found in the range 197−203 cm^{-1}. Intense peaks, both IR and Raman-active, are due to Au−S stretching modes included in the range 237−332 cm^{-1}.

3.4. $Au_{19}(SCH_3)_{13}$ Cluster. The $Au_{19}(SCH_3)_{13}$ cluster was synthesized by Jin, and its structure was proposed by Jiang.[35,36] It is formed by a defective Au_{11} core that resembles an Au_{13} icosahedron protected by two monomer and three dimer motifs. The relaxed structure has no symmetry (C_1 point group), and it is formed by 106 bonds that are included in the range 1.1−3.1 Å. Bond distances are distributed in the following manner: 39 C−H bonds (around 1.1 Å), 13 S−C bonds around 1.85 Å, 4 Au(core)−S bonds on the monomer motifs with an average distance of 2.43 Å, 4 Au(dimer)−S bonds around 2.38 Å, 12 Au(dimer)-S bonds forming the dimer motifs around 2.37 Å, and dimer motifs show an average 2.44 Å distance between Au(core) and S atoms (six distances). It is noteworthy that Au−S bonds show three different lengths with two bonds closer to 2.5 Å, as can be seen in Figure S2 in the Supporting Information. The Au_{11} core has only 22 bonds included in the range 2.75 to 3.1 Å, with the Au−Au distances being dispersed over a wide range.

dx.doi.org/10.1021/jp4033063 | J. Phys. Chem. C 2013, 117, 12191−12198

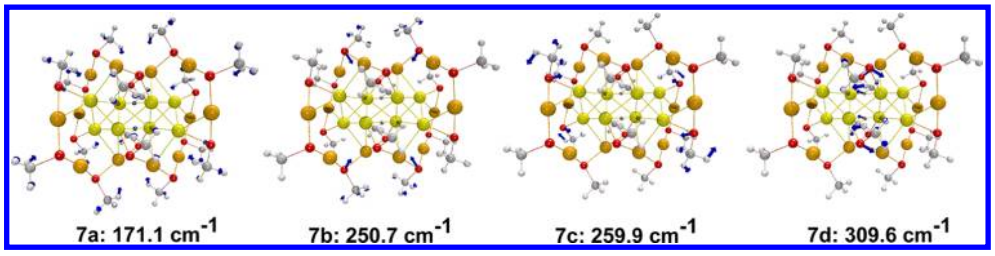

Figure 7. Selected vibrational normal modes of the $Au_{20}(SCH_3)_{16}$ cluster. S, C, H, Au(core), and Au(staple) atoms are in red, gray, white, yellow, and light brown, respectively.

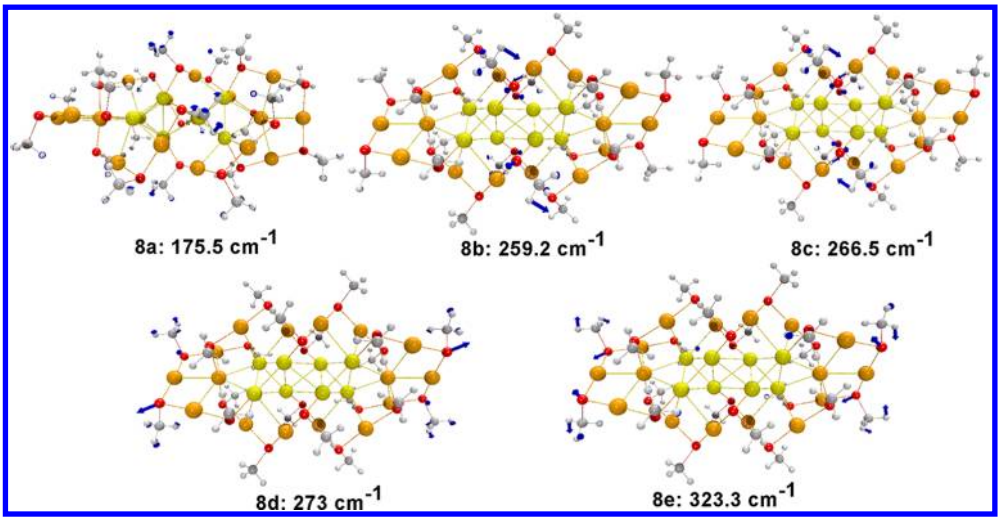

Figure 8. Selected vibrational normal modes of the $Au_{24}(SCH_3)_{20}$ cluster. S, C, H, Au(core), and Au(staple) atoms are in red, gray, white, yellow, and light brown, respectively.

The Raman spectrum of the $Au_{19}(SCH_3)_{13}$ cluster (Figure 1d) shows a major peak at 277.1 cm^{-1} due to the Au−S stretching mode of staple motifs; at 112.4 cm^{-1} the breathing mode of its Au_{11} core is identified. At 183.9 cm^{-1} is found a peak related to S-CH_3 bending mode (Figure 6a).

Regarding its IR spectrum (Figure 2d), it exhibits one intense peak at 263.7 cm^{-1} related to Au(core)−S(trimer) stretching as well as many detailed features extending to the highest at 321.9 cm^{-1} (Figure 6e), arising from a Au(trimer)−S(trimer) stretching mode. It is important to notice that the intensities of the mentioned peaks are reversed with respect to the $Au_{18}(SCH_3)_{14}$, $Au_{20}(SCH_3)_{16}$, and $Au_{24}(SCH_3)_{20}$ clusters. (See later.)

The $Au_{19}(SCH_3)_{13}$ cluster shows weak Au−S−Au modes up to 90 cm^{-1}. Torsional methyl, S−CH_3 bending, and Au−S−Au bending modes are included in the range 98−202 cm^{-1}, but more intense peaks observed at Raman and IR spectra are due to Au−S−Au bending modes. Au−S stretching modes are located in the range 241−322 cm^{-1}, accounting for the more intense peaks on IR and Raman spectra.

3.5. $Au_{20}(SCH_3)_{16}$ Cluster. The $Au_{20}(SCH_3)_{16}$ cluster was isolated by Jin et al., while its structure was proposed by Pei and coworkers in 2009.[37,38] It consists of two tetrahedral Au_4 units fused through edges, and it is covered by four trimer motifs. The relaxed structure holds a D_2 point group and is built by 120 bonds included in the range 1.1−3.1 Å. The bonds are distributed as follows: 48 C−H bonds are around 1.1 Å, 16 S−C bonds (1.85 Å), 24 Au−S bonds forming the trimer motifs (2.36 to 2.39 Å), 8 Au(core)−S bonds around 2.44 Å, 16 bonds forming the Au_8 core (2.76 to 3.1 Å) where 4 bonds are located at the fused edges (3.05 Å); the average bond distance found in Au_4 units is 2.8 Å, while the missing 8 Au(core)-Au(trimer) bonds are around 3.0 Å. As before, it is evident that Au−S bonds in the staples are slightly shorter than bonds linking staples to the Au_8 core. Given the D_2 symmetry of this $Au_{20}(SCH_3)_{16}$ cluster, it is expected that the Au−Au bonds are included in a narrow range, as can be verified in Figure S2 in the Supporting Information.

The $Au_{20}(SCH_3)_{16}$ cluster has 294 normal modes with an irreducible representation given as $\Gamma = 75A + 73B_1 + 73B_2 + 73B_3$, where A modes are Raman-active and B_1, B_2, and B_3 are both IR and Raman-active.

Its Raman spectrum (Figure 1e) shows two dominant peaks at 171.1 and 259.9 cm^{-1} (Figure 7a, 7c), which are S−CH_3 bending and Au−S stretching modes of trimer motifs, respectively. The symmetric breathing mode of the Au_8 core is located at 101.7 cm^{-1}; its low intensity is indicated by the colored stick (in Figure 1e).

The calculated IR spectrum of this cluster (Figure 2e) resembles the IR spectrum of $Au_{18}(SCH_3)_{14}$ (Figure 2c), with two main peaks located at 250.7 and 309.6 cm^{-1} (intense) (Figure 7b,d) attributable to Au−S asymmetric stretching modes.

In the $Au_{20}(SCH_3)_{16}$ cluster, vibrational normal modes up to 126 cm^{-1} are due to Au−S−Au bending modes, while in the range 128−211 cm^{-1} they are mixed with torsional methyl modes. More intense Au−S−Au bending modes are found in the range 170−207 cm^{-1}. Intense IR and Raman Au−S stretching modes are included in the range 249−337 cm^{-1}.

3.6. $Au_{24}(SCH_3)_{20}$ Cluster. It was synthesized by Jin and coworkers in 2010, and its structure was proposed by Pei and coworkers in 2012.[39,40] This structure is built by two Au_4 units

dx.doi.org/10.1021/jp4033063 | J. Phys. Chem. C 2013, 117, 12191−12198

covered by two trimer motifs and two pentamer motifs ($Au_5(SR)_6$), which are interlocked like a linked chain. A total of 144 bonds are present in the relaxed D_2 structure, with bond distances included in the range 1.1−3.1 Å. All mentioned bonds are distributed as follows: 60 C−H bonds (1.1 Å), 20 S−C bonds (1.84 Å), 12 Au(trimer)−S(trimer) bonds (2.38 Å), 4 Au(core)−S(trimer) bonds (2.47 Å), pentamer motifs showing 16 Au(pentamer)−S(pentamer) bonds (2.38 Å), 4 Au(pentamer)−S(pentamer) bonds (2.44 Å) located in the intersection plane with trimer motifs, 4 S(pentamer)−Au(core) bonds (2.43 Å), and 12 Au−S distances located in the catenation region where pentamer and trimer motifs cross with an average distance of 3.0 Å. Each Au_4 unit is formed by 6 Au(core)−Au(core) bonds of 2.79 (2), 2.8 (2), 2.83(1), and 2.88 (1) Å, respectively. All calculated Au−Au bonds are comparable to those of the $Au_{20}(SCH_3)_{16}$ cluster. (See Figure S2 in the Supporting Information.)

The $Au_{24}(SCH_3)_{20}$ cluster holds a D_2 point group and 366 vibrational normal modes given by the irreducible representation $\Gamma = 92A + 90B_1 + 92B_2 + 92B_3$.

Its Raman spectrum (Figure 1f) shows a dominant peak at 273.0 cm^{-1} (A), which is related to the symmetric Au(trimer)−S(trimer) stretching mode (Figure 8d). At 266.5 cm^{-1} Au(core)−S(pentamer) and at 246.2 cm^{-1}, Au(pentamer)−S(pentamer) stretching modes are located. The S−CH_3 bending mode is present at 175.7 cm^{-1}. A weak breathing mode is found at 86.3 cm^{-1} being shifted toward lower frequencies with respect to the other two clusters with Au_8 core clusters. This behavior was unexpected taking into account that $Au_{18}(SCH_3)_{14}$ and $Au_{20}(SCH_3)_{16}$ clusters have a similar core, but the different motifs covering the Au_8 core in $Au_{24}(SCH_3)_{20}$ might be the reason for the difference in its value. Further analysis of bond distances determined that the Au(core)−Au(core) bonds forming the $Au_{24}(SCH_3)_{20}$ cluster are shorter than bonds forming part of the $Au_{18}(SCH_3)_{14}$ and $Au_{20}(SCH_3)_{16}$ clusters.

The far-IR spectrum is dominated by features at its high-frequency end, to which the major contributing mode is an Au(trimer)−S(trimer) stretching mode at 323.3 cm^{-1}. The clearly observed IR-active S(pentamer)−Au(core) stretching modes include one at 259.2 cm^{-1}. Another pair of lower intensity peaks are attributed to S−CH_3 bending modes (160.9 cm^{-1}). Selected vibrational modes are depicted in Figure 8.

In general, the $Au_{24}(SCH_3)_{20}$ cluster shows weak Au−S−Au bending modes up to 85 cm^{-1}. Torsional methyl modes are included in the range 86−101 cm^{-1}, but they are mixed with S−CH_3 bending modes in the range 119−211 cm^{-1}. Finally, more intense IR and Raman Au−S stretching modes are located in the range 236−324 cm^{-1}.

3.7. $[Au_{25}(SCH_3)_{18}]^-$ Cluster. The anionic $Au_{25}(SCH_3)_{18}$ cluster holds a C_i symmetry, and it is formed by 137 bonds that are included in the range 1.1−3.06 Å. The Au_{13} core shows 30 bond distances in the range 2.85 to 3.06 Å. From calculated bond distances (Figures S1 and S2 in the Supporting Information) it is evident that the 12 Au−S bonds (2.47 Å) linking 6 dimer motifs to the Au_{13} core are longer than Au−S bonds found in all clusters studied. Moreover, the intra-Au_{13} bonds and the Au(core)−Au(dimer) bonds are included in several narrow ranges within the span of 2.85 to 3.29 Å. Long Au(core)−S(dimer) found in the anionic $Au_{25}(SCH_3)_{18}$ cluster might be related to the enhanced Au_{13} breathing mode observed in the experimental Raman spectra.

Vibrational normal modes of the anionic $Au_{25}(SCH_3)_{18}$ cluster have been previously reported following the irreducible representation $\Gamma = 168A_g + 171A_u$.[17] The calculated Raman spectrum (Figure 1g) shows an enhanced core Au_{13} breathing mode at 103.8 cm^{-1}, whose calculated intensity is comparable to breathing of dimer motifs located at 268.60 cm^{-1}. Another two peaks are located at 174.35 and 242.2 cm^{-1}, related to S−CH_3 bending modes and to Au−S stretching modes, respectively. The calculated frequency of the Au_{13} breathing mode is in agreement with that reported by Murray's group in 2008 (110 cm^{-1}).[11] Slight shifts in the position of Raman active peaks are inherent to the used methodology that is not taking into account the presence of counterions and, in general, the experimental conditions (ligand type, etc.). The enhancement of the Au_{13} breathing mode observed in the experimental Raman spectra may be correlated with the longer Au(core)−S(dimer) bond found in the anionic $Au_{25}(SCH_3)_{18}$ cluster, as this feature suggests an improved decoupling of core from staple-motif modes.

Calculated far-IR spectrum (Figure 2g) has a simple appearance, as it is dominated by four clear bands in the 220 to 320 cm^{-1} range. In particular, the intense broad peak centered near 240 cm^{-1} is attributed to the Au(core)−S stretching modes. In a recent paper, Tlahuice described the calculated IR spectrum covering a broader range (up to 1500 cm^{-1}) and compared its features with those observed experimentally for this and larger clusters.

Concerning the low-frequency (far-IR) spectrum, it can be generally stated that all studied thiolate-protected gold clusters show Au−S breathing modes of staple motifs in the appropriate region to explain reported experimental data: in the absorption bands found in the range 170−270 cm^{-1} (279 cm^{-1}), in a study of far-IR spectra of 2-nm alkane−thiolate-capped Au nanoparticles, as well as in the range of 220−240 cm^{-1} according to high-resolution electron energy loss spectroscopy (HREELS) studies of gold self-assembled monolayers.[14,15]

The following paragraphs summarize the obtained results.

(a) Dominant features in the far-IR spectra arise from the gold−sulfur stretching vibrations, and these are also responsible for the Raman spectral intensity at frequency shifts above ∼250 cm^{-1}. These active Au−S stretching modes may be further classified as "tangential" and "radial" according to their directionality with respect to the center. The tangential Au−S vibrations are those of the shorter, stronger bonds of the staple-motif bridges (Au(staple)−S(staple) bonds). Naturally these occur at higher frequency, typically near or above 300 cm^{-1}. The radially directed Au−S vibrations are those of the longer, "softer" bonds; these are shifted typically by about −10% with respect to the tangential modes.

(b) S−CH_3 bending vibrations (Au−S−Au bending) give rise to weaker spectral features, partially because they are spread over a much wider frequency range and their contribution to the Raman spectra is more difficult to discern (see below).

(c) Au−Au modes are nearly invisible in the far-IR spectra, in accordance with their absence of polarity, but these modes dominate the Raman spectrum at frequency-shifts $\ll$200 cm^{-1}, facilitating the detection of the incipient phonon structure of the gold-cluster cores.

Accordingly, the spectral features may be associated with the optical phonons, at high frequency ∼150 cm^{-1}, and the acoustical phonons, located at a much lower and size-sensitive frequency.

dx.doi.org/10.1021/jp4033063 | J. Phys. Chem. C 2013, 117, 12191−12198

Important among the latter are the "breathing" (totally symmetric expansion−contraction of the core) and the quadrupolar deformation mode. Impulsive excitation of these modes by short laser pulses has been found to generate oscillations that may be detected in real time by ultrafast optical spectroscopy.[41]

The calculated frequencies of seven thiolate-protected gold clusters studied colored in according with type of vibrational normal modes are depicted in Figure 9.

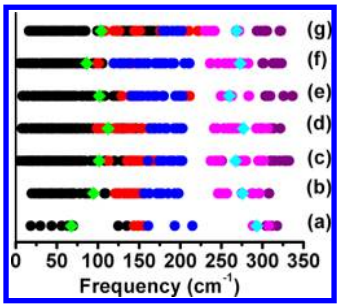

Figure 9. Classification of the calculated vibrational normal modes. (a) $Au_4(SCH_3)_4$, (b) $[Au_{12}(SCH_3)_9]^+$, (c) $Au_{18}(SCH_3)_{14}$, (d) $Au_{19}(SCH_3)_{13}$, (e) $Au_{20}(SCH_3)_{16}$, (f) $Au_{24}(SCH_3)_{20}$, and (g) $[Au_{25}(SCH_3)_{18}]^-$. Au−S−Au bending, torsional methyl, S-CH_3 bending, tangential Au−S, radial Au−S, core breathing, and staples breathing modes are shown in black, red, blue, purple, pink, green, and cyan, respectively.

4. CONCLUSIONS

This report has addressed the study of the structures and vibrational normal modes of well-established thiolate-protected gold clusters with 4, 12, 18, 19, 20, 24, and 25 Au atoms on the basis of DFT calculations. Their calculated Raman spectra show distinctive patterns characteristic to each cluster size, whereas it is not easy to discern a size-dependent trend in the frequencies of the breathing mode of both the core and staple motifs. In general, Raman spectra show more intense peaks attributed to breathing mode of the staple motifs, while the anionic $Au_{25}(SCH_3)_{18}$ cluster shows an enhanced core-breathing intensity that might be related to long Au−S bonds linking the dimer motifs to the Au_{13} core. We conclude that cationic $Au_{12}(SCH_3)_9$ and $Au_{20}(SCH_3)_{24}$ clusters show the more intense peaks for the breathing modes of staple motifs, while the anionic $Au_{25}(SCH_3)_{18}$ cluster shows the more intense Au_{13} breathing mode of all studied structures.

The calculated IR spectra show an interesting feature for the clusters having Au_8 cores; the more intense peak appears around 325 cm^{-1}, while for the clusters with Au_{11} and Au_{13} cores this maximum shifts toward lower frequencies approximately located near 240 cm^{-1}. The calculated IR spectrum of $Au_{18}(SCH_3)_{14}$ shows two intense peaks that are attributed to Au−S asymmetric stretching modes of dimer and trimer motifs.

The calculated IR and Raman spectra reported herein, along with the interpretation of the trends found in the spectra, are intended to encourage new experimental studies and to assist in their interpretation. In particular, the promise of high information content spectra should help to justify higher resolution experimental work in the low-frequency region, which may require sample cooling (to remove thermal broadening and population effects), special optics in Raman spectrometers to discriminate against the Rayleigh line, and competing luminescence from the clusters with broadband absorption in the visible and near-IR regions as well as coherent radiation sources (synchrotron, free-electron, or terahertz (THz) devices) and time-domain (femtosecond) spectroscopic methods.

■ ASSOCIATED CONTENT

Supporting Information

Bond distances of all studied clusters in two different ranges. Comparison of various ligands attached to tetramer and Au_{25} clusters and their effect on bond lengths and symmetric normal modes frequencies. This material is available free of charge via the Internet at http://pubs.acs.org.

■ AUTHOR INFORMATION

Corresponding Author

*E-mail: tlahuicef@gmail.com. Tel: (210) 458 8173.

Notes

The authors declare no competing financial interest.

■ ACKNOWLEDGMENTS

A. T.-F. acknowledges Consejo Nacional de Ciencia y Tecnología (CONACyT) and the Departamento de Supercómputo of Universidad Nacional Autónoma de México and the National Science Fundation (NSF) for support with grants DMR-1103730, "Alloys at the Nanoscale: The Case of Nanoparticles Second Phase" and PREM: NSF PREM Grant # DMR 0934218; "Oxide and Metal Nanoparticles- The Interface Between Life Sciences and Physical Sciences".

■ REFERENCES

(1) Daniel, M. C.; Astruc, D. Gold Nanoparticles: Assembly, Supramolecular Chemistry, Quantum-Size-Related Properties, and Applications toward Biology, Catalysis, and Nanotechnology. *Chem. Rev.* **2004**, *104*, 293−346.

(2) Shaw, C. F., III. Gold-Based Therapeutic Agents. *Chem. Rev.* **1999**, *99*, 2589−2600.

(3) Jadzinsky, P. D.; Calero, G.; Ackerson, C. J.; Bushnell, D. A.; Kornberg, R. D. Structure of a Thiol Monolayer-Protected Gold Nanoparticle at 1.1 Å Resolution. *Science* **2007**, *318*, 430−433.

(4) Akola, J.; Walter, M.; Whetten, R. L.; Häkkinen, H.; Grönbeck, H. On the Structure of Thiolate-Protected Au_{25}. *J. Am. Chem. Soc.* **2008**, *130*, 3756−3757.

(5) Zhu, M.; Aikens, C. M.; Hollander, F. J.; Schatz, G. C.; Jin, R. Correlating the Crystal Structure of A Thiol-Protected Au_{25} Cluster and Optical Properties. *J. Am. Chem. Soc.* **2008**, *130*, 5883−5885.

(6) Heaven, M. W.; Dass, A.; White, P. S.; Holt, K. M.; Murray, R. W. Crystal Structure of the Gold Nanoparticle $[N(C_8H_{17})_4][Au_{25}(SCH_2CH_2Ph)_{18}]$. *J. Am. Chem. Soc.* **2008**, *130*, 3754−3755.

(7) Lopez-Acevedo, O.; Tsunoyama, H.; Tsukuda, T.; Häkkinen, H.; Aikens, C. M. Chirality and Electronic Structure of the Thiolate-Protected Au_{38} Nanocluster. *J. Am. Chem. Soc.* **2010**, *132*, 8210−8218.

(8) Qian, H.; Eckenhoff, W. T.; Zhu, Y.; Pintauer, T.; Jin, R. Total Structure Determination of Thiolate-Protected Au_{38} Nanoparticles. *J. Am. Chem. Soc.* **2010**, *132*, 8280−8281.

(9) Pei, Y.; Zeng, X. C. Investigating the Structural Evolution of Thiolate Protected Gold Clusters from First-Principles. *Nanoscale* **2012**, *4*, 4054−4072.

(10) Gruene, P.; Rayner, D. M.; Redlich, B.; van der Meer, A. F. G.; Lyon, J. T.; Meijer, G.; Fielicke, A. Structures of Neutral Au_7, Au_{19}, and Au_{20} Clusters in the Gas Phase. *Science* **2008**, *321*, 674−676.

(11) Parker, J. F.; Choi, J. P.; Wang, W.; Murray, R. W. Electron Self-Exchange Dynamics of the Nanoparticle Couple $[Au_{25}(SC_2Ph)_{18}]^{0/1-}$ By Nuclear Magnetic Resonance Line-Broadening. *J. Phys. Chem. C* **2008**, *112*, 13976−13981.

(12) Miller, S. A.; Womick, J. M.; Parker, J. F.; Murray, R. W.; Moran, A. M. Femtosecond Relaxation Dynamics of $Au_{25}L_{18}^-$ Monolayer-Protected Clusters. *J. Phys. Chem. C.* **2009**, *113*, 9440−9444.
(13) Qian, H.; Sfeir, M. Y.; Jin, R. Ultrafast Relaxation Dynamics of $[Au_{25}(SR)_{18}]^q$ Nanoclusters: Effects of Charge State. *J. Phys. Chem. C* **2010**, *114*, 19935−19940.
(14) Petroski, J.; Chou, M.; Creutz, C. The Coordination Chemistry of Gold Surfaces: Formation and Far-Infrared Spectra of Alkanethiolate-Capped Gold Nanoparticles. *J. Organomet. Chem.* **2009**, *694*, 1138−1143.
(15) Nuzzo, R. G.; Zegarski, B. R.; Dubois, L. H. Fundamental Studies of the Chemisorption of Organosulfur Compounds on Gold(111). Implications for Molecular Self-Assembly on Gold Surfaces. *J. Am. Chem. Soc.* **1987**, *109*, 733−740.
(16) Akola, J.; Kacprzak, K. A.; Lopez-Acevedo, O.; Walter, M.; Grönbeck, H.; Häkkinen, H. Thiolate-Protected Au_{25} Superatoms as Building Blocks: Dimers and Crystals. *J. Phys. Chem. C* **2010**, *114*, 15986−15994.
(17) Tlahuice-Flores, A. Normal Modes of $Au_{25}(SCH_3)_{18}^-$, $Ag_{12}Au_{13}(SCH_3)_{18}^-$, and $Ag_{25}(SCH_3)_{18}^-$ Clusters. *Mol. Simul.* **2013**, *39*, 428−431.
(18) Perdew, J. P.; Burke, K.; Ernzerhof, M. Generalized Gradient Approximation Made Simple. *Phys. Rev. Lett.* **1996**, *77*, 3865−3868.
(19) (a) Jiménez-Hoyos, C. A.; Benjamin, J. G.; Scuseria, G. E. Evaluation of Range-Separated Hybrid Density Functionals for the Prediction of Vibrational Frequencies, Infrared Intensities, And Raman Activities. *Phys. Chem. Chem. Phys.* **2008**, *10*, 6621−6629. (b) Merrick, J. P.; Moran, D.; Radom, L. An Evaluation of Harmonic Vibrational Frequency Scale Factors. *J. Phys Chem. A.* **2007**, *111*, 11683−11700.
(20) Frisch, M. J.; Trucks, G. W.; Schlegel, H. B.; Scuseria, G. E.; Robb, M. A.; Cheeseman, J. R.; et al. *Gaussian 03*, revision B.03; Gaussian.; Inc.: Wallingford, CT, 2003
(21) Bau, R. Crystal Structure of the Antiarthritic Drug Gold Thiomalate (Myochrysine): A Double-Helical Geometry in the Solid State. *J. Am. Chem. Soc.* **1998**, *120*, 9380−9381.
(22) LeBlanc, D. J.; Lock, C. J. L. Cyclo-Hexakis[(2,4,6-triisopropylthiophenolato-S:S)gold(I)] Diethyl Ether Solvate. *Acta Crystallogr., Sect. C* **1997**, *53*, 1765−1768.
(23) Wiseman, M. R.; Marsh, P. A.; Bishop, P. T.; Brisdon, B. J.; Mahon, M. F. Homoleptic Gold Thiolate Catenanes. *J. Am. Chem. Soc.* **2000**, *122*, 12598−12599.
(24) (a) Grönbeck, H.; Walter, M.; Häkkinenm, H. Theoretical Characterization of Cyclic Thiolated Gold Clusters. *J. Am. Chem. Soc.* **2006**, *128*, 10268−10275. (b) Kacprzak, A. K.; Lopez-Acevedo, O.; Häkkinen, H.; Grönbeck, H. Theoretical Characterization of Cyclic Thiolated Copper, Silver, and Gold Clusters. *J. Phys. Chem. C* **2010**, *114*, 13571−13576.
(25) Simpson, C. A.; Farrow, C. L.; Tian, P.; Billinge, S. J. L.; Huffman, B. J.; Harkenss, K. M.; Cliffel, D. E. Tiopronin Gold Nanoparticle Precursor Forms Aurophilic Ring Tetramer. *Inorg. Chem.* **2010**, *49*, 10858−10866.
(26) Barngrover, B. M.; Aikens, C. M. Electron and Hydride Addition to Gold(I) Thiolate Oligomers: Implications for Gold−Thiolate Nanoparticle Growth Mechanisms. *J Phys. Chem. Lett.* **2011**, *2*, 990−994.
(27) Jiang, D. E.; Whetten, R. L.; Luo, W.; Dai, S. The Smallest Thiolated Gold Superatom Complexes. *J. Phys. Chem. C* **2009**, *113*, 17291−17295.
(28) Zhang, Y.; Shuang, S.; Dong, C.; Lo, C.-K.; Paau, M.-C.; Choi, M. M. F. Application of HPLC and MALDI-TOF MS for Studying As-Synthesized Ligand-Protected Gold Nanoclusters Products. *Anal. Chem.* **2009**, *81*, 1676−1685.
(29) Tlahuice, A.; Garzón, I. L. Structural, Electronic, Optical, And Chiroptical Properties of Small Thiolated Gold Clusters: The Case of Au_6 and Au_8 Cores Protected with Dimer $[Au_2(SR)_3]$ and Trimer $[Au_3(SR)_4)]$ Motifs. *Phys. Chem. Chem. Phys.* **2012**, *14*, 7321−7329.
(30) Negishi, Y.; Nobusada, K.; Tsukuda, T. Glutathione-Protected Gold Clusters Revisited: Bridging the Gap between Gold(I)-Thiolate Complexes and Thiolate-Protected Gold Nanocrystals. *J. Am. Chem. Soc.* **2005**, *127*, 5261−5270.
(31) Negishi, Y.; Takasugi, Y.; Sato, S.; Yao, H.; Kimura, K.; Tsukuda, T. Kinetic Stabilization of Growing Gold Clusters by Passivation with Thiolates. *J. Phys. Chem. B.* **2006**, *110*, 12218−12221.
(32) Shichibu, Y.; Negishi, Y.; Tsunoyama, H.; Kanehara, M.; Teranishi, T.; Tsukuda, T. Extremely High Stability of Glutathionate-Protected Au25 Clusters Against Core Etching. *Small* **2007**, *3*, 835−839.
(33) Reilly, S. M.; Krick, T.; Dass, A. Surfactant-Free Synthesis of Ultrasmall Gold Nanoclusters. *J. Chem. Phys. C.* **2010**, *114*, 741−745.
(34) Tlahuice, A.; Garzón, I. L. On the Structure of The $Au_{18}(SR)_{14}$ Cluster. *Phys. Chem. Chem. Phys.* **2012**, *14*, 3737−3740.
(35) Wu, Z.; MacDonald, M. A.; Chen, J.; Zhang, P.; Jin, R. Kinetic Control and Thermodynamic Selection in the Synthesis of Atomically Precise Gold Nanoclusters. *J. Am. Chem. Soc.* **2011**, *133*, 9670−9673.
(36) Jiang, D. E. Staple Fitness: A Concept To Understand and Predict the Structures of Thiolated Gold Nanoclusters. *Chem.—Eur. J.* **2011**, *17*, 12289−12293.
(37) Zhu, M.; Qian, H.; Jin, R. Thiolate-Protected Au_{20} Clusters with a Large Energy Gap of 2.1 eV. *J. Am. Chem. Soc.* **2009**, *131*, 7220−7221.
(38) Pei, Y.; Gao, Y.; Zeng, X. C. Thiolate-Protected $Au_{20}(SR)_{16}$ Cluster: Prolate Au_8 Core with New $[Au_3(SR)_4]$ Staple Motif. *J. Am. Chem. Soc.* **2009**, *131*, 13619−13621.
(39) Zhu, M.; Qian, H.; Jin, R. Thiolate-Protected $Au_{24}(SC_2H_4Ph)_{20}$ Nanoclusters: Superatoms or Not? *J. Phys. Chem. Lett.* **2010**, *1*, 1003−1007.
(40) Pei, Y.; Pal, R.; Liu, C.; Gao, Y.; Zhang, C.; Zeng, X. C. Interlocked Catenane-Like Structure Predicted in $Au_{24}(SR)_{20}$: Implication to Structural Evolution of Thiolated Gold Clusters from Homoleptic Gold(I) Thiolates to Core-Stacked Nanoparticles. *J. Am. Chem. Soc.* **2012**, *134*, 3015−3024.
(41) Sauceda, H. E.; Mongin, D.; Maioli, A. C.; Pellarin, M.; Del Fatti, N.; Vallée, F.; Garzón, I. L. Vibrational Properties of Metal Nanoparticles: Atomistic Simulation and Comparison with Time-Resolved Investigation. *J. Phys. Chem. C.* **2012**, *116*, 25147−25156.